AIAA JOURNAL
Vol. 34, No. 3, March 1996

Free Shear Layer Interaction with an Expansion-Compression Wave Pair

Mahadevan Ramaswamy,* Eric Loth,† and J. Craig Dutton‡
University of Illinois at Urbana–Champaign, Urbana, Illinois 61801

Experiments were performed using high-speed cinematography to spatially and temporally resolve compressible planar mixing layer structures in pressure matched and unmatched conditions. The unmatched conditions (overexpanded and underexpanded) were achieved by enforcing a static pressure difference between the supersonic planar jet exit ($M \sim 1.65$) and the ambient quiescent flow below. The pressure mismatch resulted in the interaction of expansion-compression waves with the free shear layer. Temporally resolved planar images, autocorrelations, and temporal correlations were obtained for a portion of the flowfield just downstream of the expansion-compression interaction. The results showed increased fluctuations in shear layer structure angles for the unmatched pressure conditions as compared with those for the matched condition. The degree of angular fluctuations qualitatively correlated with a nondimensional pressure gradient parameter, and the time scale was consistent with the eddy passage frequency. The passive scalar convection speeds for the unmatched conditions were found to be significantly lower than for the matched cases.

I. Introduction

THERE has been extensive research on incompressible planar mixing layers, for which the self-similar growth rate was found to be a function of the low-speed to high-speed density and velocity ratios (λ_ρ and λ_u), and whose behavior was typified by well-organized predominantly two-dimensional spanwise vortical structures. There have also been extensive recent experimental, computational, and theoretical efforts to understand the physics of compressible turbulent mixing layers because of their implications in separated base flows, scramjets, chemical lasers, thermal sprays, etc. For example, experimental findings of Papamoschou and Roshko,[1] Goebel and Dutton,[2] and Samimy et al.[3] have noted strong changes in the fundamental character of the flow due to compressibility, resulting in turbulence anisotropy and reduction in growth rates when compared with the incompressible case of comparable freestream density and velocity ratios. Clemens and Mungal[4] also showed that the large-scale structures, which control the bulk of mass entrainment and turbulence, become highly three dimensional as compressibility increases.

The aforementioned changes are typically characterized by the convective Mach number, which was initially suggested by Bogdanoff[5] as the parameter to decouple the compressibility effects from the density and velocity ratios for supersonic mixing. The isentropic convective Mach number of each of the freestreams is derived based on the assumption of stagnation pressure balance at the saddle point between two large-scale structures and by assuming an isentropic stagnation process. For the flows considered herein, the specific heat ratios of both streams are the same; therefore the theoretical isentropic convective Mach number satisfies the relation $M^i_{c,1} = M^i_{c,2} = M^i_c$, and the theoretical isentropic convective velocity of the large-scale structures (U^i_c) can be found from the formula

$$U^i_c = \frac{U_1 + U_2\sqrt{\lambda_\rho}}{\sqrt{\lambda_\rho} + 1} \tag{1}$$

where λ_ρ is the low-speed to high-speed density ratio; M is the Mach number; U is the velocity; the subscripts 1, 2, and c represent the high-speed flow, low-speed flow, and the convection speed, respectively; and the superscript i represents the theoretical isentropic case.

Determining convection speeds experimentally is difficult for high-speed flows. Tracking a specific feature of a structure over schlieren frames to find the convective speed[6] may introduce subjectiveness due to the three-dimensionality and evolution of these structures with time. Also, choosing a feature that is close to either the higher or lower speed stream may give a biased result about the convective speed. One way to obtain convection speeds is through digital image processing of planar passive scalar images. The spatial covariance of the mixture fraction intensity field in the mixing layer reveals the size and orientation of large-scale structures in the mixing layer,[7,8] and the temporal covariance gives the scalar convective speed of the structure as it convects downstream.[9] These covariances can be obtained by statistical analysis of the digitized planar Mie scattering results and provide an average convection speed across the shear layer. Papamoschou[6] and Dimotakis[10] noted that schlieren-based results generally agree with a stream selection rule: $M_{c,2} > M_{c,1}$ when one stream is supersonic and the other subsonic, and $M_{c,2} < M_{c,1}$ for both streams supersonic. On the other hand, two-point correlations from velocity or pressure probes can be used to obtain the convection speed at a particular transverse location. Using a variety of these techniques, there have been several studies of the large-structure convection speed in compressible shear layers that yielded conflicting results.

A survey of these investigations by Ramaswamy[11] revealed that the techniques for determining U_c generally fall into two categories: 1) those based on correlation of the temporally resolved flow visualizations of a nominally passive scalar field throughout the shear layer, e.g., density gradient via shadowgraph[10] or schlieren imaging,[6,12,13] or flow seeding via passive entrainment,[9] product formation,[14] or planar laser-induced fluorescence,[15] all of which yielded various U_c almost always consistent with the speed selection rule[10]; and 2) those based on two-point correlations of momentum-based variables at particular transverse locations, e.g., measurements of velocity via hot-wire probes[16] or pressure via fast response static pressure probes,[3] all of which yielded various U_c nearly equal to the isentropic value at the centerline of the mixing layer and a transverse distribution of the measured U_c consistent with previous incompressible shear layer results.[17] In addition, DNS[18] and inviscid eddy simulations[19] both show that the cores (minimum pressure points) and braids (maximum pressure points) move at nearly the isentropic convection speed even at high convective Mach numbers. These results indicate that for compressible mixing layers the structures identified by passive scalar techniques may in general

Received Aug. 22, 1994; revision received April 12, 1995; accepted for publication May 18, 1995.

*Postdoctoral Research Associate, Department of Mechanical and Industrial Engineering. Member AIAA.
†Associate Professor, Department of Aeronautical and Astronautical Engineering. Senior Member AIAA.
‡Professor, Department of Mechanical and Industrial Engineering. Associate Fellow AIAA.

move at a different speed than those identified by momentum-based variables.

Gas dynamic interactions with turbulence, e.g., shock waves[20] and expansion waves,[21] have also received significant attention. More specifically for experimental planar compressible shear layers, Menon[22] observed that significant increases in shear layer growth rate occurred when subjected to a combination of expansion and oblique shock waves. In addition, Shau et al.[23] found experimentally that a two oblique shock interaction essentially eliminated growth rate for approximately five shear layer thicknesses δ downstream of the interaction initiation, followed by an enhanced growth rate for five more δ, after which the shear layer growth returned to its original unperturbed rate and extrapolated thickness. In Shau's study, the structures were also noticed to flatten towards the streamline direction during the low-growth-rate region, to become more vertical during the high-growth period, and then to return to the intermediate angle of their undisturbed counterparts. Finally, Hall et al.[24] recently mentioned experimental results where unmatched pressure conditions (causing shock and expansion waves) led to enhanced growth rate and possible structure modification.

Based on the preceding discussion, there is some evidence that gas dynamic waves can affect the coherent structure dynamics in a compressible mixing layer. However, the nature and details of such an interaction in compressible shear layers with unmatched pressure conditions is not well understood. Therefore, the focus of this research is to examine the dynamics of the shear layer large-scale passive scalar structures when subjected to expansion-compression wave interaction using passive scalar cinematography. This work represents the first temporally resolved study of such a flow interaction and includes results of structure dynamics as well as convection speeds.

II. Experimental Methods

A. Flow Facility and Test Conditions

The experimental facility used in this study is a single stream planar supersonic wind tunnel run at both matched and unmatched conditions.[9] The dimensions of the single stream nozzle exit are 50 mm wide by 13.5 mm high with a uniform exit Mach number of ~1.65 (verified with pitot surveys). The lower wall of the single stream supersonic wind tunnel extends only to the splitter plate tip, with a trailing-edge thickness of 0.1 mm. The subsequent rectangular test section measures 100 mm long and 50 mm wide, with the bottom open to allow the entrainment of ambient air. The flow facility consists of high-pressure nitrogen supply from six conventional high-pressure tanks. The test conditions in terms of ambient pressure p_0, nozzle exit pressure p_e, framing rate, and theoretical convective Mach number for all cases are shown in Table 1. Note, tests cases with an M indicate matched conditions, with an O indicate overexpanded conditions, and with a U indicate underexpanded conditions.

The present study employs a light sheet Mie scattering visualization technique to provide two-dimensional planar transverse views of the large-scale structures present in the mixing layer. This technique is similar to that of Clemens and Mungal[4] and has been extended to cinematography by Mahadevan and Loth.[9] The technique involves visualization of a passive scalar (alcohol), which is seeded far upstream in the high-speed flow with a mass fraction of approximately 0.9%. As this evaporated mixture expands through the wind-tunnel nozzle, alcohol condenses into a fine fog of submicron droplets. These drops act as the tracer particles for the high-speed fluid in the test section and indicate the extent of low-speed fluid entrainment in the mixing layer.[9] Details of droplet formation, equilibrium size, etc., are given by Ramaswamy.[11]

The light source unit used is a Xenon Model 519 micropulse system operated at 200 J/pulse at a nominal square pulse duration of 25 μs. The light source functions as an effective overall shutter, exposing several frames of the film through a single pulse, and produces a light sheet approximately 50 mm wide with a thickness of 5.5 mm at the mixing layer. The supersonic mixing layer images are documented by a Beckman–Whitley Model 192 Continuous Writing Framing Camera with 35-mm film. The image transmission and shuttering are based on the Miller principle, which stabilizes the image for each frame and is accomplished by a two-lens system between the rotating mirror and the frames. Shutter exposure time is approximately one-half the framing rate that leads to a corresponding amount of image blur. Details of the image blur and the Stokes number of the alcohol condensate are documented in Ref. 9. The images captured on Kodak 35-mm T-max 3200 ASA black and white film were boost developed at around 18,000 ASA using a T-max developer.

B. Digital Image Processing

To extract global information from the resulting images, digital processing and statistical analysis were employed to enhance the quality of the images and to obtain spatial and temporal correlations. The 8-bit (gray scale) digitization of the film prints typically yielded a 750 × 350 spatial matrix over the 30 × 14 mm image domain. Since the intensity of scattered light is proportional to the alcohol droplet density, the 8-bit intensity index gives a qualitative indication of the alcohol mixture fraction f. Note that a row corresponds to pixels along the streamwise direction x, and a column corresponds to pixels along the transverse direction y.

To correct for intensity variations in the streamwise direction caused by nonuniform illumination, the intensity index $I(x, y)$, of each column was thresholded based on the average intensity of the extremum values, first above and then below the mixing layer, and the difference stretched to a range of 0–255. This process was repeated for all frames, thus eliminating interframe lighting variations. The spatial covariance and temporal covariance are determined using

$$C(\Delta x, \Delta y) = \frac{1}{N}\sum_{1}^{N} I'(x^* + \Delta x, y^* + \Delta y) I'(x^*, y^*) \quad (2)$$

$$C(\Delta x, \Delta y, \Delta t) = \frac{1}{N}\sum_{1}^{N} I'(x^* + \Delta x, y^* + \Delta y, t + \Delta t) I'(x^*, y^*, t) \quad (3)$$

Table 1 Test conditions

Case no.	p_0, atm	p_e, atm	Δt, μs[a]	U_1, m/s	$M_1/M_2/M_c^i$	$(dp/dx)^b_{rms}$	x, mm[c]
Matched							
M1	0.96	0.96	2.91	470	1.67/0/0.74	0	45
M2	0.97	0.99	2.40	470	1.67/0/0.74	0	45
M3	0.98	0.97	2.77	457	1.67/0/0.74	0	27
Overexpanded							
O1	0.96	0.75	2.88	441.7	1.52/0/0.70	0.30	46
O2	0.96	0.75	2.80	441.7	1.52/0/0.70	0.30	46
O3	0.97	0.73	2.85	437.7	1.50/0/0.69	0.36	46
O4	0.98	0.84	2.91	447.4	1.57/0/0.71	0.21	46
Underexpanded							
U1	0.97	1.18	2.77	491.7	1.81/0/0.81	0.47	47
U2	0.98	1.16	2.71	478.8	1.78/0/0.79	0.47	47

[a]Time between adjacent frames based on inverse of framing speed.
[b]Pressure gradient: nondimensionalized with respect to ambient pressure and shear layer thickness.
[c]Streamwise, distance from splitter plate for start of the interrogation region.

where

$$I'(x, y) = \bar{I}(y) - I(x, y) \tag{4}$$

where I' represents the intensity fluctuation based on the row mean, the point (x^*, y^*) represents the pixel location with respect to which the covariance was computed (in this study all points in the interrogation area were considered), and N represents the total number of offset points $(\Delta x, \Delta y)$ that were used for correlation for each (x^*, y^*), within the interrogation area. The streamwise convection speed U_c can be determined by noting the displacement Δx at which the temporal correlation is maximized, $\Delta x_{\max,c}$, and dividing it by the interframe time Δt. Structure angles were estimated based on the major axis of the 0.5 correlation contour, and eccentricity was taken as unity minus the ratio of major to minor axis (associated uncertainties in these quantities are discussed by Ramaswamy[11]).

The uncertainty associated with the present measurements for a single frame convection velocity determination U_c was based on a 95% confidence level (approximated as twice the standard deviation). The factors that contribute to this uncertainty include 1) digital pixel resolution, 2) dependence on interrogation area, and 3) image blur caused by the acceleration of structures during the frame exposure period (details discussed in Ramaswamy[11]). The digitization and image resolution uncertainty was the largest of the three and was estimated as 6% of U_c. Interrogation area dependence contributed to a 2.5% uncertainty level. The structure blur uncertainty was estimated by using a Taylor series expansion in time of a fluid particle convecting during the frame exposure (about 1.25 μs), which yielded a 4% uncertainty based on evolution of structures at the Taylor microscale. Thus, the total uncertainty of U_c associated with any frame pair is 7.5%. However, the uncertainty of the present time-averaged convection velocity $\bar{U}_c$ with respect to one obtained with large time histories for a given case is significantly higher since it was based on a limited number of frame pairs, e.g., four. The uncertainty in $\bar{U}_c$ was estimated based on the number of samples and the average standard deviation within a set of samples, yielding an overall uncertainty for $\bar{U}_c$ of 18% for each sequence. Although this is significant, it will be shown that the differences between matched and unmatched conditions consistently exceed this margin. In addition, basing the average on several sequences (cases) that are at the same condition, e.g., O1 and O2, will reduce this uncertainty accordingly.

C. Characterization of Pressure Mismatch

The specific interest of this study was the interaction of an expansion-compression wave pair with the mixing layer. This was achieved with both underexpanded and overexpanded exit conditions, such that the area of interrogation includes an expansion-compression interaction and the immediate downstream flow development (Figs. 1a and 1b). Note that all flows in this paper are presented as moving from left to right with the high-speed stream above. Before the results are presented, a characterization of the degree of pressure mismatch is given to help interpret the subsequent findings. To do this, we consider the gas dynamic perturbations experienced by a shear layer structure as it passes through the expansion-compression interaction. An expansion wave reflecting from the top wall will reflect downwards as an expansion wave as well. However, upon impingement on the approximately constant pressure sonic line contour of the shear layer, it will reflect upwards as a compression wave. Note that if we assume quasisteady structure convection, the pressure variations caused by the structure itself, e.g., low pressure in the core and high pressure in the braid, will be steady with respect to the structure and thus should not be considered as a perturbation.

Therefore, the effect of an Eulerian steady wave pattern such as shown in Fig. 1 on the shear layer turbulence passing through the expansion-compression interaction (and above the sonic line) would be a pressure decrease followed by a pressure increase of equal but opposite strength. Thus, the net streamwise pressure gradient (dp/dx) through both waves is zero, but the rms of the streamwise pressure gradient is not. We may define its nondimensional strength $(dp/dx)_{\text{rms}}$ by normalizing this gradient with the quiescent stream pressure (which is constant) divided by the average local shear layer thickness δ_f (see Table 1), where δ_f is the transverse distance between $\bar{f} = 0.9$ and 0.1. The latter locations were determined by the normalized intensity index obtained from the processed Mie scattering images. We might expect $(dp/dx)_{\text{rms}}$ to be an additional controlling parameter along with M_c, λ_u, λ_ρ, etc. Note that as the wall height increases for a constant shear layer thickness,

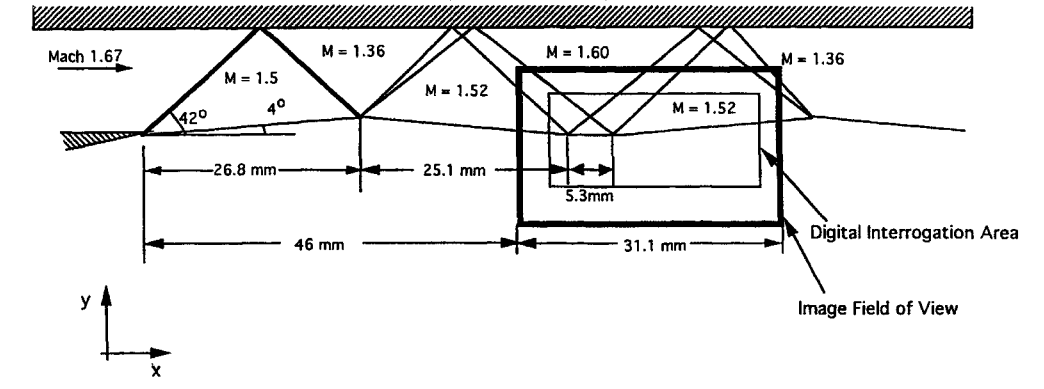

a) Overexpanded

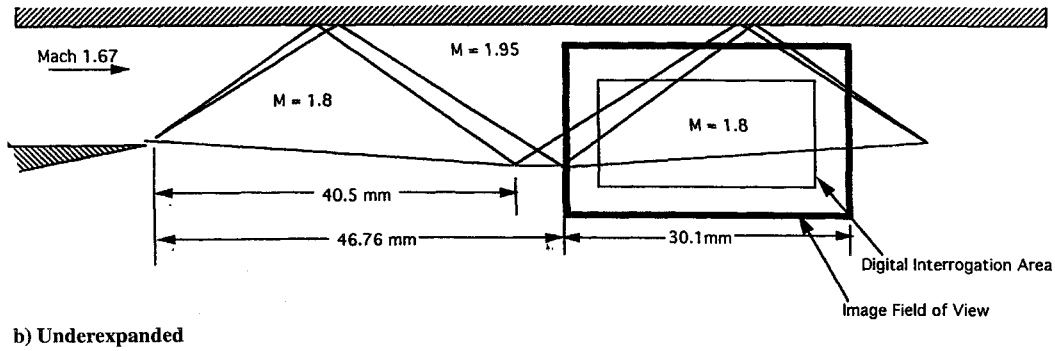

b) Underexpanded

Fig. 1 Typical interrogation area with respect to steady gasdynamics.

this normalized perturbation will decrease (see Fig. 1) due to the increase in interaction length.

The gas dynamic pattern of Fig. 1 can be significantly modified by the shear layer turbulence through acoustic feedback such as the jet screech as noted by Tam,[25] which can, in turn, affect the large-scale structure convection. However, detailed acoustic measurements by Ramaswamy[11] indicated that the addition of two acoustically reflective surfaces was necessary to accomplish this excitation, and such configurations were not used for the present measurements.

III. Results and Discussion

Figure 2 shows a single frame of the shear layer for case O2 as well as a close-up sequence for a selected portion of the flow. To better illustrate the large-scale structures, a consistent single threshold level based on a mean intensity has been applied to the original gray scale image used for covariance statistics. The white region above corresponds to the high-speed fluid, whereas the darker region below corresponds to the entrained quiescent air. Although distinct structures in the shear layer are visible, their evolution and orientation are not well organized compared with those found in the subsonic case,[26] which is consistent with several previous studies as mentioned earlier. The general lack of spatial coherency of the mixing layer structures suggests the existence of three dimensionality as noted in the endwise spatially resolved images of Clemens and Mungal.[4] Fingerlike protrusions of ambient air into the supersonic stream and vice versa are visible as has been previously observed for the mixing layer under matched pressure conditions.[8,9] But in the unmatched pressure cases, we observe that fluctuations in the angular orientation of the structures are more pronounced compared

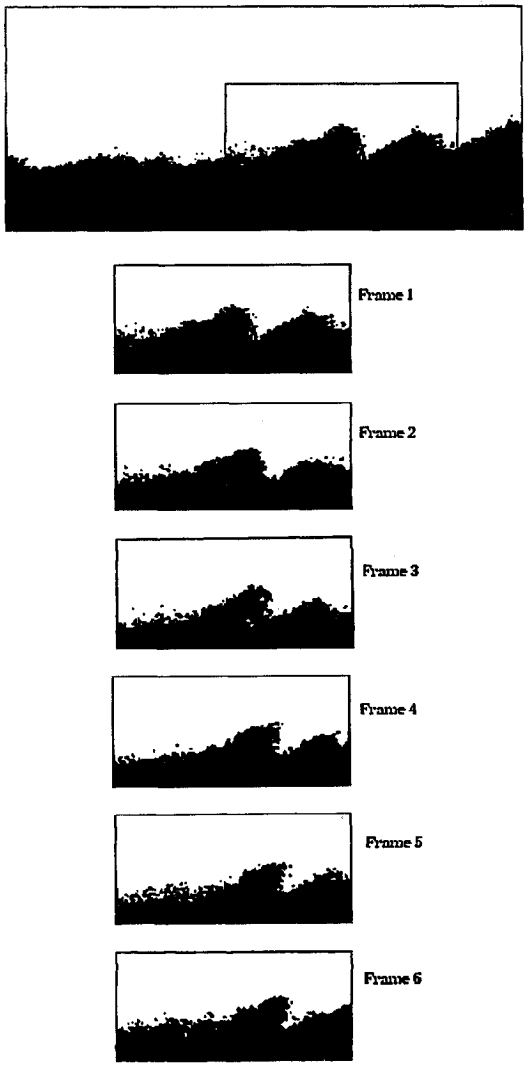

Fig. 2 Mie scattering movie of case O2.

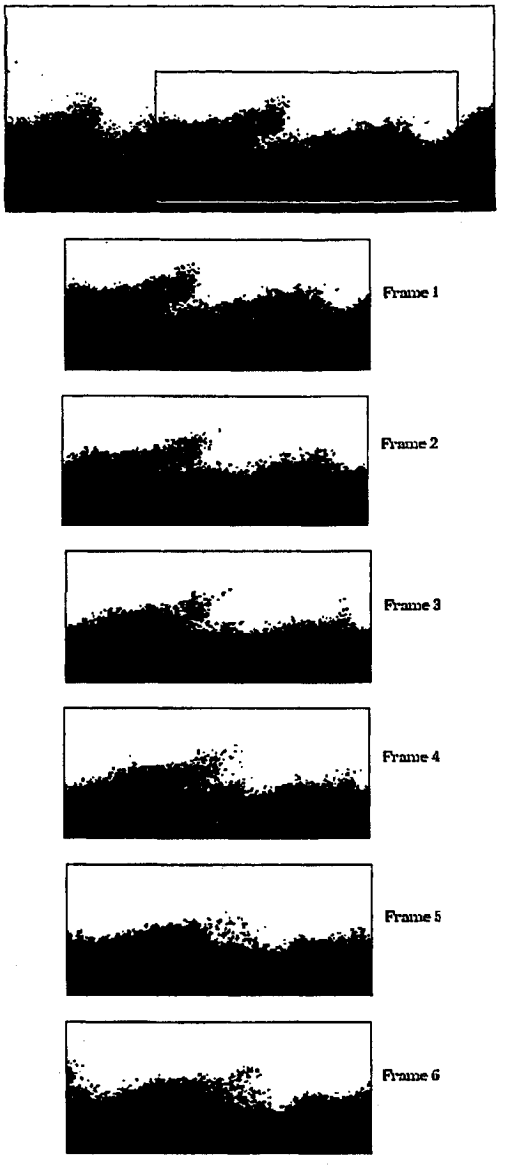

Fig. 3 Mie scattering movie of case O4.

with the matched pressure cases, as will be shown by the spatial covariance calculations.

In the sequence in Fig. 2, the newly developing dark structure protruding upward in the center of frame 1 is seen to generally become thinner and elongated as it tilts toward the streamwise axis while it convects downstream. On the other hand, Fig. 3 (also at unmatched conditions) shows the reduction of coherency of a similar structure that is already elongated in frame 1. Although such structures tend to retain coherency over the framing duration of 15 μs, typically they rise initially upwards from the streamwise direction and then begin to fall towards the streamwise direction and lose coherency as they convect downstream. In general, this was the most common structure evolution observed in all of the unmatched sequences (e.g., Figs. 2 and 3). The structures under matched pressure conditions also exhibited similar evolutions but were less frequent and less pronounced.[9] In either case, we do not see the classical rotational pairing as commonly observed with the incompressible case; in fact, the image sequences obtained here support the modified merging mechanism of slapping, whereupon the upstream structures impact the downstream structure without significant transverse (rotational) movement. This slapping mechanism was noted in the spatially evolving computations of Oh and Loth[19] and found to be more dominant as the convective Mach number increased.

Figure 4 shows autocorrelations for several frames based on a pressure matched sequence (M1). From these plots, the average normalized structure size based on the ratio of the major axis (at

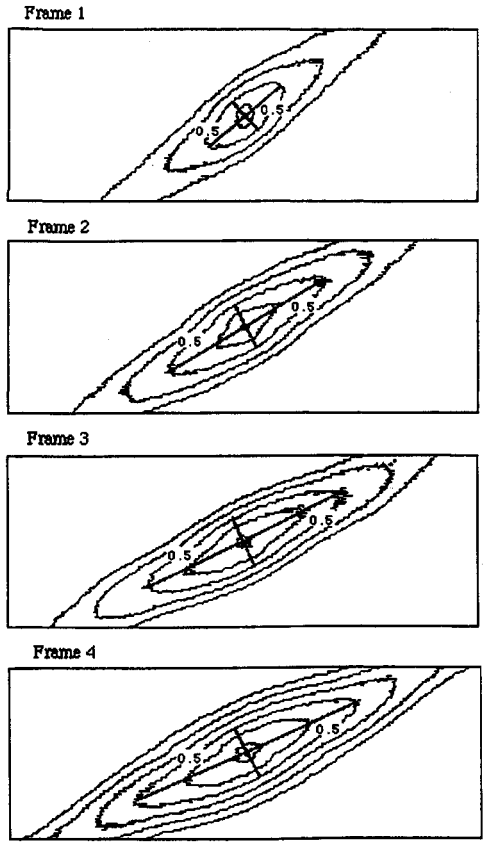

Fig. 4 Autocovariance of case M4 frames (center of each box corresponds to $\Delta x, \Delta y = 0, 0$).

a correlation contour level of 0.5) to the mixture fraction mixing layer thickness δ_f was found to be about 1.5. The average angular orientation of the structure with respect to the local mean flow direction was measured to be approximately 26.5 deg with a measured eccentricity of 0.55. We note that the size, orientation, and shape of the structures are roughly constant with respect to time for this condition, indicating quasisteady convection. Other pressure matched cases yielded similar quasisteady results.

Several sequential autocorrelations for an overexpanded flow case (O2) are shown in Fig. 5. We find that the angle, size, and shape change significantly during the sequence for the unmatched cases, as compared with the matched cases. Note that as new structures are generated in the interrogation area, the orientation of the covariance is expected to shift away from the streamwise direction, and as the structure convects downstream, the orientation of the covariance will tilt back towards the streamwise direction due to actual tilting of the structures themselves. Since the interrogation area typically contained the same two or three large structures for a sequence, their net structural evolution with time can be noted from the covariance evolution.

The time evolutions of the angular orientation of the autocorrelation for some of the sequences are shown in Fig. 6, where $t = 0$ simply corresponds to the first frame of a sequence, and each subsequent frame appears as a data point. Here one can clearly note that, as compared with the matched cases, the unmatched sequences generally exhibit a larger average angle (44 vs 21 deg) as well as a larger standard deviation about each case's average structure angle (7.7 vs 2.6 deg). In general, the larger angles for the unmatched cases seen in Fig. 6 are consistent with results from Shau et al.[23] for the initial downstream effect of oblique shock interaction. However, the average shape (as given by the eccentricity) and size is nearly the same for matched and unmatched conditions (Table 2), although large variations were again noted. Strong changes in the angular orientation of the structure with time are noted in Fig. 6 for cases O1 and O2 (with the same test conditions), due to well-defined vertical protrusions of the ambient air entraining into the shear layer. These increased fluctuations qualitatively correspond to the larger values of $(dp/dx)_{rms}$ of these cases (see Table 1). Note that case

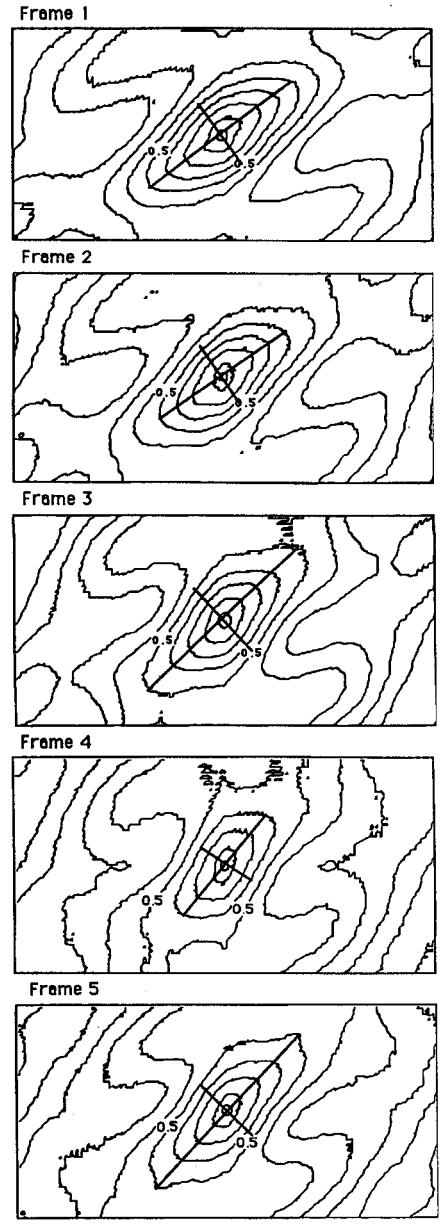

Fig. 5 Autocovariance of case O2 frames (center of each box corresponds to $\Delta x, \Delta y = 0, 0$).

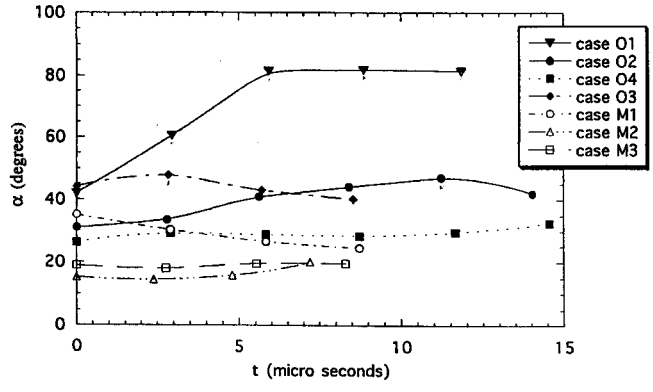

Fig. 6 Angular orientation of structure vs time.

O4 is only slightly overexpanded, i.e., it has a lower $(dp/dx)_{rms}$ as compared with the other cases and tends to show a steadier behavior of the structure angle with time, similar to the matched conditions. The time scale (eddy roll over time) of the shear layer, τ_δ, may be approximated as 15 μs basing the typical eddy size in the shear layer on a δ_f of 7 mm and a velocity difference of about 470 m/s. The

Table 2 Experimental results

Case no.	$\bar{U}_c$, m/s	σ of $\bar{U}_c$, %[a]	U_c^i, m/s	M_{c1}, exp	M_{c2}, exp	Eccentricity	δ_f, mm[b]
Matched							
M1	350	0.79	258	0.43	1.02	0.71	7.3
M2	354	8.2	258	0.41	1.03	0.35	8.5
M3	375	5.6	250	0.3	1.1	0.62	3.7
Overexpanded							
O1	151	12.8	239	1.0	0.44	0.41	9.6
O2	165	41.0	239	0.94	0.48	0.6	7.2
O3	157	41.0	237	0.97	0.5	0.43	5.4
O4	224	26.0	243	0.78	0.66	0.58	6.0
Underexpanded							
U1	236	30.0	273	0.94	0.69	0.57	7.3
U2	256	22.0	271	0.85	0.75	0.34	7.2

[a]% standard deviation σ of U_c normalized with the average U_c.
[b]Shear layer thickness based on mixture fraction.

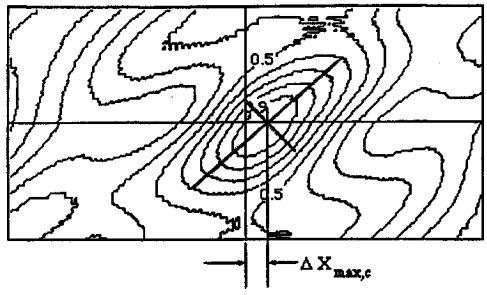

Fig. 7 Averaged temporal covariance of case O2 sequence.

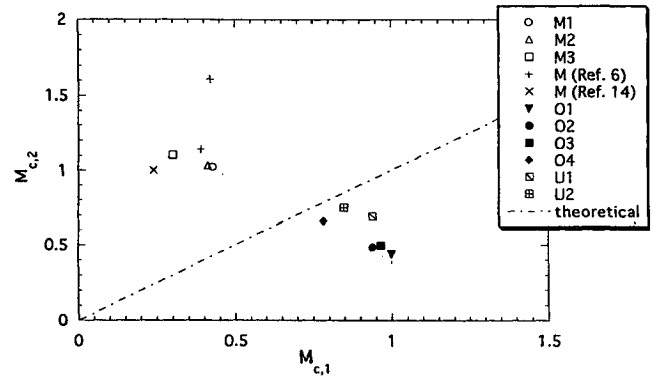

Fig. 8 Experimental vs theoretical (isentropic) convective Mach number for supersonic-subsonic flows.

time scale of the resulting angular fluctuations is also expected to be on the order of τ_δ, which is consistent with Fig. 6.

An average temporal covariance for case O2 was obtained by correlating each of the five successive frame pairs and averaging the result, shown as a contour plot in Fig. 7. Here we note a shape similar to the average of the spatial correlations of case O2 shown in Fig. 5, which is consistent with a uniform convection of the structures. Note that the window of interrogation of a frame sequence may include both tilting of existing structures as they convect and generation of new structures at higher angles to the streamwise direction, such that there are both positive and negative deviations from an average angle.

The average convective speed of the structures obtained from these temporal covariances is tabulated for all cases in Table 2, along with their standard deviation. In general, the unmatched cases have a much larger standard deviation for $\bar{U}_c$ despite the similarity in the signal-to-noise ratio of the images. This deviation is consistent with the increased structure variability of the unmatched conditions. Based on the wave patterns shown in Fig. 1, the local high-speed fluid velocity U_1 in the interrogation region was computed. Combined with the experimentally determined $\bar{U}_c$, the convective Mach numbers $M_{c,1}$ and $M_{c,2}$ were then calculated and plotted in Fig. 8, where the isentropic counterparts for each case are simply equal to the theoretical convective Mach number M_c^i given in Table 1. We will first address the results of the matched condition convection speeds, for which results from two other matched condition studies[6,14] with supersonic-subsonic flow conditions are also shown.

Results of the present matched condition cases and those of Refs. 6 and 14 agree well with the "stream selection rule," i.e., $M_{c,2} > M_{c,1}$, which is consistent with other scalar/density-based convection results.[11] In contrast, the results for the unmatched conditions show a significant reduction in $\bar{U}_c$ (i.e., $M_{c2} < M_{c1}$), which is opposite of the speed selection rule; see Table 2 and Fig. 8. The consistency of the underexpanded and overexpanded results in this regard is presumably due to the commonality of the expansion-compression interaction noted in Figs. 1a and 1b. Note that case O4, which has a reduced pressure gradient perturbation, also has a reduced departure from the theoretical value of M_c^i. Based on the discussion for matched condition convective speeds, we may attempt to explain the reduction in $\bar{U}_c$ for the unmatched conditions as follows. The higher convective speeds obtained with the matched conditions imply that the large-scale structures visualized with Mie scattering or other passive scalar measurements will have stronger correlations above the mean velocity line. However, the expansion-compression interaction may significantly modify the shear layer dynamics such that the passive scalar structures have stronger correlations below the mean velocity line (which is approximately equal to both the sonic and isentropic convection lines). This modification could be the result of shock cell oscillations that may 1) cause strong entrainment asymmetry, i.e., ingestion of a large fraction of the low-speed stream's mass into the shear layer, or 2) preferentially reduce temporal coherency of structures on the high-speed side, i.e., structures above the sonic line are more variable and short lived than the quasisteady convection below, causing a shift of the temporal correlation peak toward the low-speed stream.

We may also consider the temporal correlations of transverse segments of the passive scalar images to note possible changes in convection speed along the transverse direction. Recall that passive scalar-based techniques typically provide U_c based on the entire shear layer thickness, whereas two-point correlations give the convection speed at a specific transverse location.[11] Figure 9 shows the result of the sequence-averaged $\bar{U}_c$ values where points within a specific segment were correlated only with points in a corresponding segment of the adjacent frame for both matched and unmatched cases. The results show that the local passive scalar convection speeds also have significant transverse variations as seen for their momentum-based counterparts.[3,16] In addition, we note that for the matched case, the transverse position of the mean velocity ($U_1/2$) location is below that based on mean scalar intensity level, indicating a preferential entrainment of high-speed fluid (this difference is consistent with recent numerical results[19]). The unmatched cases show the opposite effect, indicating preferential entrainment of low-speed fluid, which is consistent with aforementioned mechanism 1. Finally, we note a lack of data for some of the higher transverse positions of the unmatched cases. This is due to very low signal-to-noise ratios for autocorrelations at these locations, which is consistent with

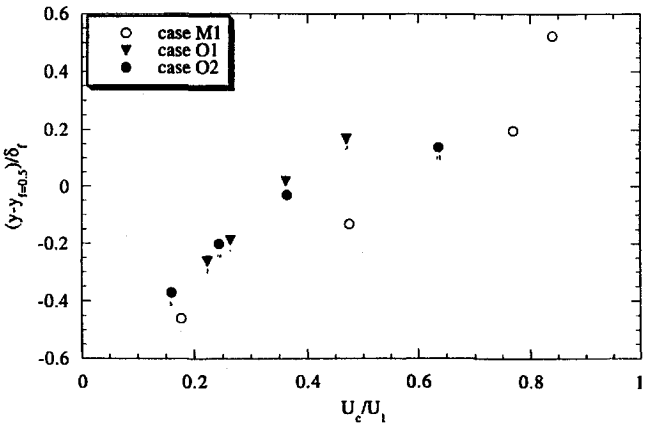

Fig. 9 Convection speed variation across shear layer.

a reduction in coherency above the sonic line that biases the convection speed to the more highly correlated low-speed side, as suggested in aforementioned mechanism 2. In fact, the reduction in coherency in the high-speed part of the shear layer for unmatched cases is likely to lead to reduction in entrainment in these regions, i.e., mechanism 2 may lead to mechanism 1. However, the preceding observations may be limited to supersonic-subsonic shear layers, for which the steady gas dynamic wave influence on the turbulence is constrained to be primarily above the sonic line. Obviously, more work is needed to determine the fundamental mechanism for the reduction in U_c for the unmatched cases.

IV. Conclusions

Digital analysis of the Mie scattering results from the pressure mismatched experiments showed that expansion-compression wave interaction with the shear layer caused both stronger fluctuations and an increase in the angular orientation of the large-scale structures in the shear layer. These were related to the more volatile eddy dynamics as compared with results from matched conditions, especially as the strength of the pressure mismatch increases. Convection speeds for the pressure matched conditions based on the Mie scattering results followed the stream selection rule, as was also found for several previous passive scalar- or density-based convection studies. However, the convective speeds of the structures obtained from the pressure mismatched conditions were found to be less than the isentropic speeds, opposite of the result expected from the stream selection rule developed for the matched pressure conditions. It is postulated that the passive scalar perturbations were more correlated below the mean velocity line (i.e., more likely to convect in a quasisteady manner) for the unmatched cases, as opposed to above the mean velocity line for the matched case.

References

[1]Papamoschou, D., and Roshko, A., "The Compressible Turbulent Shear Layer: An Experimental Study," *Journal of Fluid Mechanics*, Vol. 197, Dec. 1988, pp. 453–477.

[2]Goebel, S. G., and Dutton, J. C., "Experimental Study of Compressible Turbulent Mixing Layers," *AIAA Journal*, Vol. 29, No. 4, 1991, pp. 538–546.

[3]Samimy, M., Elliot, G. S., and Reeder, M. F., "Compressibility Effects on Large Structures in Free Shear Flows," Eighth Symposium on Turbulent Shear Flows, Technical Univ. of Munich, Germany, Sept. 1991.

[4]Clemens, N. T., and Mungal, M. G., "Two- and Three-Dimensional Effects in the Supersonic Mixing Layer," *AIAA Journal*, Vol. 30, No. 4, 1992, pp. 973–981.

[5]Bogdanoff, D. W., "Compressibility Effects in Turbulent Shear Layers," *AIAA Journal*, Vol. 21, No. 6, 1983, pp. 926, 927.

[6]Papamoschou, D., "Structure of the Compressible Turbulent Shear Layer," AIAA Paper 89-0126, 1989.

[7]Long, M. B., Chu, B. T., and Chang, R. K., "Instantaneous Two-Dimensional Gas Concentration Measurements by Light Scattering," *AIAA Journal*, Vol. 19, No. 9, 1981, pp. 1151–1157.

[8]Messersmith, N. L., "An Experimental Investigation of Organized Structures and Mixing in Compressible Turbulent Free Shear Layers," Ph.D. Thesis, Univ. of Illinois at Urbana–Champaign, Urbana, IL, 1992.

[9]Mahadevan, R., and Loth, E., "High-Speed Cinematography of Compressible Mixing Layers," *Experiments in Fluids*, Vol. 17, 1994, pp. 179–189.

[10]Dimotakis, P. E., "On the Convection Velocity of Turbulent Structures in Supersonic Shear Layers," AIAA Paper 91-1724, June 1991.

[11]Ramaswamy, M., "Gas Dynamic and Acoustic Interactions with Supersonic Free Shear Layers," Ph.D. Thesis, Univ. of Illinois at Urbana–Champaign, Urbana, IL, 1994.

[12]Lepicovsky, J., Ahuja, K. K., Brown, W. H., and Burrin, R. H., "Coherent Large-Scale Structures in High Reynolds Number Supersonic Jets," *AIAA Journal*, Vol. 25, No. 11, 1987, pp. 1419–1425.

[13]McIntyre, S. S., and Settles, G. S., "Optical Experiments on Axisymmetric Compressible Turbulent Mixing Layers," AIAA Paper 91-0623, 1991.

[14]Fourguette, D. C., Mungal, M. G., and Dibble, R. W., "Time Evolution of the Shear Layer of a Supersonic Axisymmetric Jet," *AIAA Journal*, Vol. 29, No. 7, 1991, pp. 1123–1130.

[15]Bunyajitradulya, A., and Papamoschou, D., "Acetone PLIF Imaging of Turbulent Shear-Layer Structure at High Convective Mach Number," AIAA Paper 94-0617, 1994.

[16]Barre, S., Quine, C., and Dussauge, J. P., "Compressibility Effects on the Structure of Supersonic Mixing Layers: Experimental Results," *Journal of Fluid Mechanics*, Vol. 259, March 1994, pp. 47–78.

[17]Batt, R. G., "Turbulent Mixing of Passive and Chemically Reacting Species in a Low-Speed Shear Layer," *Journal of Fluid Mechanics*, Vol. 82, Aug. 1977, pp. 53–95.

[18]Lele, S. K., "Direct Numerical Simulation of Compressible Free Shear Flows," AIAA Paper 89-0374, 1989.

[19]Oh, C. K., and Loth, E., "Unstructured Grid Simulations of Spatially Evolving Supersonic Shear Layers," *AIAA Journal*, Vol. 33, No. 7, 1995, pp. 1229–1238.

[20]Lele, S. K., "Shock-Jump Relations in a Turbulent Flow," *Physics of Fluids A*, Vol. 4, No. 12, 1992, pp. 2900–2905.

[21]Li, C., Kailasanath, K., and Book, D. L., "Mixing Enhancement by Expansion Waves in Supersonic Flows of Different Densities," *Physics of Fluids A*, Vol. 3, No. 5, 1991, pp. 1369–1373.

[22]Menon, S., "Shock-Wave-Induced Mixing Enhancement in Scramjet Combustors," AIAA Paper 89-0104, 1989.

[23]Shau, Y. R., Dolling, D. S., and Choi, K. Y., "Organized Structure in a Compressible Turbulent Shear Layer," *AIAA Journal*, Vol. 31, No. 8, 1993, pp. 1398–1405.

[24]Hall, J. L., Dimotakis, P. E., and Rosemann, H., "Experiments in Non-Reacting Compressible Shear Layers," *AIAA Journal*, Vol. 31, No. 12, 1993, pp. 2247–2253.

[25]Tam, C. K. W., "On Broad Band Shock Associated Noise of Supersonic Jets," *Recent Advances in Aeroacoustics, Proceedings of International Symposium*, edited by A. Krothapalli and C. A. Smith, Stanford Univ., Stanford, CA, 1993.

[26]Brown, G. L., and Roshko, A., "On Density Effects and Large Structures in Turbulent Mixing Layers," *Journal of Fluid Mechanics*, Vol. 64, July 1974, pp. 775–816.